

This work was written as part of one of the author's official duties as an Employee of the United States Government and is therefore a work of the United States Government. In accordance with 17 U.S.C. 105, no copyright protection is available for such works under U.S. Law.

Public Domain Mark 1.0

<https://creativecommons.org/publicdomain/mark/1.0/>

Access to this work was provided by the University of Maryland, Baltimore County (UMBC) ScholarWorks@UMBC digital repository on the Maryland Shared Open Access (MD-SOAR) platform.

**Please provide feedback**

Please support the ScholarWorks@UMBC repository by emailing [scholarworks-group@umbc.edu](mailto:scholarworks-group@umbc.edu) and telling us what having access to this work means to you and why it's important to you. Thank you.



Published in final edited form as:

*Appl Opt.* 2017 May 10; 56(14): 4105–4112.

## Equivalence of internal and external mixture schemes of single scattering properties in vector radiative transfer

Lipi Mukherjee<sup>1</sup>, Peng-Wang Zhai<sup>1,\*</sup>, Yongxiang Hu<sup>2</sup>, and David M. Winker<sup>2</sup>

<sup>1</sup>Department of Physics, University of Maryland Baltimore County, Baltimore, Maryland 21250, USA

<sup>2</sup>MS 475 NASA Langley Research Center, Hampton, Virginia 23681-2199, USA

### Abstract

Polarized radiation fields in a turbid medium are influenced by single-scattering properties of scatterers. It is common that media contain two or more types of scatterers, which makes it essential to properly mix single-scattering properties of different types of scatterers in the vector radiative transfer theory. The vector radiative transfer solvers can be divided into two basic categories: the stochastic and deterministic methods. The stochastic method is basically the Monte Carlo method, which can handle scatterers with different scattering properties explicitly. This mixture scheme is called the external mixture scheme in this paper. The deterministic methods, however, can only deal with a single set of scattering properties in the smallest discretized spatial volume. The single-scattering properties of different types of scatterers have to be averaged before they are input to deterministic solvers. This second scheme is called the internal mixture scheme. The equivalence of these two different mixture schemes of scattering properties has not been demonstrated so far. In this paper, polarized radiation fields for several scattering media are solved using the Monte Carlo and successive order of scattering (SOS) methods and scattering media contain two types of scatterers: Rayleigh scatterers (molecules) and Mie scatterers (aerosols). The Monte Carlo and SOS methods employ external and internal mixture schemes of scatterers, respectively. It is found that the percentage differences between radiances solved by these two methods with different mixture schemes are of the order of 0.1%. The differences of  $Q/I$ ,  $U/I$ , and  $V/I$  are of the order of  $10^{-5} \sim 10^{-4}$ , where  $I$ ,  $Q$ ,  $U$ , and  $V$  are the Stokes parameters. Therefore, the equivalence between these two mixture schemes is confirmed to the accuracy level of the radiative transfer numerical benchmarks. This result provides important guidelines for many radiative transfer applications that involve the mixture of different scattering and absorptive particles.

### OCIS codes

(010.5620) Radiative transfer; (290.1310) Atmospheric scattering; (260.5430) Polarization; (350.5500) Propagation; (120.7000) Transmission

---

\*Corresponding author: pwzhai@umbc.edu.

## 1. INTRODUCTION

The radiative transfer equation (RTE) governs the transfer of radiation field in a turbid medium, which has important applications in a variety of scientific fields such as astrophysics, remote sensing, climate science, and many more [1–4]. A turbid medium in radiative transfer processes consists of particles that may absorb, emit, and scatter radiation fields. In realistic applications, a turbid medium may contain two or more kinds of scattering particles. In atmospheric radiative transfer, scattering particles include molecules, aerosols, and cloud droplets. In ocean optics, scattering particles include phonons (pressure fluctuations), viruses, phytoplankton, and many other constituents [5]. Each kind of particle has different inherent optical properties, and it is critical to properly determine the scattering properties of a mixed turbid medium from those of each individual constituent.

The common practice to mix scattering properties of two or more scattering particles is to average them using optical depths as weighting factors [see Eqs. (4)–(6) in Section 2]. Hereafter, we refer to this approach as the internal mixture scheme (IMS). IMS is a necessary step before one can solve the RTE using deterministic methods, which discretize the spatial domain with only one set of scattering properties allowed for a specific location. In other words, one has to specify a unique value for each of the scattering properties (scattering and extinction coefficients, scattering matrix). A noncomplete list of deterministic numerical methods includes the discrete-ordinate (DISORT) [1,6–15], invariant embedding [16–20], adding and doubling [21–23], matrix operator [24–31], spherical harmonics [32–34], spherical harmonics discrete ordinate [35,36], and successive order of scattering (SOS) methods [37–49].

The stochastic method, i.e., the Monte Carlo (MC) method, can handle more than one kind of scattering particle at a specific location, without using IMS [50–57]. If there are two or more kinds of scattering particles, the MC method can use random processes to determine which kind of scattering particle interacts with radiation upon a scattering event. Specifically, a random number is compared with relative scattering probabilities to select a scattering particle. The phase function of the selected particle is then used to sample the scattered direction. This procedure, described in Section 2.C in detail, is referred to as the external mixture scheme (EMS). Despite its wide usage, the equivalence of IMS and EMS has not yet been directly proved or verified. In this paper, we demonstrate this equivalence by comparing the solutions of the RTE using two methods. One is the SOS method, which uses IMS [48,49]; the other is the MC code, which uses EMS [50].

This paper is organized as follows: Section 2 outlines the vector RTE and explains IMS and EMS; Section 3 describes two radiative transfer cases used for comparison, shows the simulation results, and demonstrates the equivalence of IMS and EMS; Section 4 summarizes the conclusions reached in this study.

## 2. THEORY

### A. RTE

A beam of light with arbitrary polarization may be represented by the Stokes vector  $\mathbf{L} = (I, Q, U, V)^T$ , where the four elements  $I$ ,  $Q$ ,  $U$ , and  $V$  are the Stokes parameters; the superscript  $T$  stands for the transpose of the vector. As a beam of light propagates through a medium, it experiences absorption, emission, and scattering processes. These interactions are mathematically described by the RTE [1,2,5,6,58,59], which has the following form for the plane-parallel condition without thermal emission [1,6,60]:

$$\mu \frac{d\mathbf{L}(\tau, \mu, \phi)}{d\tau} = \mathbf{L}(\tau, \mu, \phi) - \mathbf{S}(\tau, \mu, \phi), \quad (1)$$

where  $\tau$  is the optical depth defined as the product of the extinction coefficient  $\beta$ , and the vertical path length;  $\mu = \cos(\theta)$  and  $\theta$  is the viewing zenith angle;  $\phi$  is the viewing azimuthal angle. All the zenith angles in this paper are defined with respect to the upward direction.  $\theta < 90^\circ$  means that the direction is pointing upward and  $\theta > 90^\circ$  when pointing downward. Figure 1 is the solar and viewing geometry with two detectors shown: one is at the top of the atmosphere (TOA), measuring the reflected Stokes parameters; the other is at the bottom of the atmosphere (BOA), measuring the transmitted Stokes parameters.

The source matrix  $\mathbf{S}$  is

$$\mathbf{S}(\tau, \mu, \phi) = \frac{\omega(\tau)}{4\pi} \int_0^{2\pi} \int_{-1}^1 \mathbf{P}(\tau, \mu, \phi, \mu', \phi') \cdot \mathbf{L}(\tau, \mu', \phi') d\mu' d\phi', \quad (2)$$

where  $\omega = \beta_s/\beta_e$  is the single-scattering albedo and  $\beta_s$  is the scattering coefficient. Equation (2) is valid in a macroscopically isotropic and mirror symmetric medium [3].  $\mathbf{P}$  is the planetary form of the phase matrix defined as [61]

$$\mathbf{P}(\tau, \mu, \phi, \mu', \phi') = \mathbf{R}(\pi - i_2) \cdot \mathbf{F}(\tau, \Theta) \cdot \mathbf{R}(-i_1). \quad (3)$$

The rotation matrix  $\mathbf{R}$  rotates the reference plane of the Stokes vector between the meridian and scattering planes;  $i_1$  and  $i_2$  are the rotation angles [1,62];  $\mathbf{F}$  is the scattering matrix for the turbid medium; the scattering angle  $\Theta$  is a function of variables  $\mu, \phi, \mu', \phi'$ .

In the RTE, the scattering matrix and scattering albedo depend on geometric shapes, indices of refraction, and inhomogeneities of scattering particles. When two or more types of scattering particles are present, the scattering properties of the mixture have to be properly determined. In the following, we describe the two mixture schemes: IMS and EMS.

## B. IMS

There are basically two kinds of numerical methods to solve the vector RTE: the deterministic and stochastic methods. The deterministic method treats each discretized spatial domain with a single set of scattering properties. If scattering media consist of more than one kind of scatterer, the IMS is employed.

Here the scattering medium is assumed to consist of two kinds of scatterers: molecules and aerosols. Their optical properties are averaged using the optical depths as weighting factors

$$\mathbf{P}_{\text{mix}} = \frac{\tau_{sr}\mathbf{P}_r + \tau_{sa}\mathbf{P}_a}{\tau_{sr} + \tau_{sa}}, \quad (4)$$

where  $\tau_{sr}$  and  $\tau_{sa}$  are the scattering optical depths of Rayleigh and aerosol particles, respectively.  $\mathbf{P}_r$  and  $\mathbf{P}_a$  are the phase matrices of Rayleigh and aerosol particles, respectively. The total optical depth  $\tau_{\text{mix}}$  of the mixed medium is

$$\tau_{\text{mix}} = \tau_{er} + \tau_{ea}, \quad (5)$$

where  $\tau_{er}$  and  $\tau_{ea}$  are the extinction optical depths of Rayleigh and aerosol particles, respectively.

The effective single scattering albedo of the mixed medium is

$$\omega_{\text{eff}} = \frac{\tau_{sr} + \tau_{sa}}{\tau_{er} + \tau_{ea}}. \quad (6)$$

After scattering properties are mixed using Eqs. (4)–(6), they are used as the inputs to the deterministic radiative transfer solver to calculate the vector radiation field. In this paper, the deterministic numerical method used is the SOS code for coupled atmosphere and ocean systems [48]. In this method, the total radiance vector is expressed as a summation of contributions from photons scattered a number of times, from 0 to a maximum number of  $N$  [38,46,63,64]

$$\mathbf{L}(\tau, \mu, \phi) = \sum_{n=1}^N \mathbf{L}_n(\tau, \mu, \phi). \quad (7)$$

For single scattering, there exists an analytical solution and the second-order scattering contribution can be found by integrating the single-scattering contribution. Each higher-order scattered field can be iteratively calculated from a radiation field of one less order of scattering. This procedure is repeated until the remainder can be either ignored or approximated by a geometric series. It has been found that the maximum scattering order of 40 satisfies most practical applications [49]. The Delta- $m$  [65] or Delta-fit [48,66] is used to truncate the phase functions with elongated forward-scattering peaks. The truncated

scattering matrices are then expanded in terms of the spherical harmonics in order to obtain the Fourier expansion of the phase matrices. This procedure is described in Refs. [48,67], and also called sphFT in Ref. [68]. A solution to the RTE is then found using the Fourier expansion of the phase matrices. To compensate for the error introduced by these truncation schemes, the single-scattering contribution is corrected by an analytical solution using an untruncated original phase function [69]. The iteration of source matrix method is used to calculate the Stokes parameters  $I$ ,  $Q$ ,  $U$ ,  $V$  at arbitrary viewing angles [70,71]. Recently, the inelastic Raman scattering for ocean water has been included in the vector radiative transfer solution [72]. Originally developed for coupled atmosphere and ocean systems, the code can also be configured to calculate the radiation field for atmosphere and land systems. The SOS code has been carefully validated against benchmark data for atmosphere and surface systems [60,73] and other independent radiative transfer codes, for instance, the adding method by Chowdhary *et al.* [74].

### C. EMS

In the EMS, scattering properties of different scatterers are not mixed in the same fashion as IMS. Instead, a random process is used by the MC method to select a scatterer upon each scattering event. EMS is closely related to the MC method, so we will start with a brief introduction to this method and emphasize how EMS is implemented.

The stochastic model to solve the RTE is the MC method [55,57,75–77], which emulates the behavior of photons propagating in a turbid medium. The MC code used in this study was developed by Zhai *et al.* [50] for solving vector radiative transfer in a three-dimensional medium, which can also be used to simulate radiative transfer in one-dimensional plane parallel systems. The MC code has been validated with benchmark results [60,73]. This method initializes a photon package with location and direction determined by a light source, which is assumed to be the solar radiation in this study. Then the optical depth that the photon package can propagate through before a scattering event can happen is determined by

$$\tau = -\ln(\xi), \quad (8)$$

where  $\xi$  is a random number uniformly distributed between 0 and 1. The photon is then moved to its new location, with propagation length determined by

$$d = \tau / \beta_e, \quad (9)$$

where  $\beta_e = \beta_r + \beta_a$  is the total extinction coefficient,  $\beta_r$  and  $\beta_a$  are the extinction coefficients of Rayleigh and aerosol particles, respectively. This equation is valid only in a homogenous medium. For a three-dimensional inhomogeneous medium, the distance  $d$  has to be determined in a stepwise manner as described in Zhai *et al.* [50]. Next, a new random number is used to determine which scatterer is responsible for this scattering event. Assuming  $\xi'$  is a new random number, if

$$0 \leq \xi' \leq \beta_r / (\beta_r + \beta_a), \quad (10)$$

molecules are responsible for this scattering event. If

$$\beta_r / (\beta_r + \beta_a) \leq \xi' \leq 1, \quad (11)$$

aerosols are the active agents that interact with the photon package. To handle absorptions, the weight of the photon package is multiplied by the single-scattering albedo of selected scattering particles. The scattering matrix of selected particles is then used to estimate the detector radiation response and sample scattered direction. For detailed documentation of how this MC code works, readers are referred to Zhai *et al.* [50]. In the end, the polarized radiation field is output for a medium with multiple types of scatterers. The procedure of selecting scattering particles from Eqs. (10) to (11) is called EMS in this study.

### 3. SIMULATION AND DISCUSSION

To test the equivalence of IMS and EMS outlined above, two cases are designed: one with a conservative scattering medium, the other with gas absorption included. The conservative case is a mixture of molecules and aerosols. The scattering matrix of molecules is the Rayleigh scattering matrix, and the aerosol scattering matrix is calculated by the Mie theory [67]. The molecular extinction optical depth is  $\tau_{er} = 0.3186$ , which is the molecular optical depth at  $\lambda = 0.412 \mu\text{m}$  for the Earth's atmosphere [78]. The aerosol optical depth is  $\tau_{ea} = 0.3262$ , which is a typical value for aerosol optical depth [60]. In general, the Rayleigh and aerosol optical depths are a function of wavelength [79]. However, the equivalence of IMS and EMS does not depend on the relative proportional of the two scatterers, which means that there is no need to repeat simulations with different combinations of Rayleigh and aerosol optical depths.

The aerosol model used is the same as in Kokhanovsky *et al.* [60], and an aerosol of radius  $a$  is assumed to follow the lognormal distribution

$$f(a) = \frac{1}{\sqrt{2\pi}sa} \exp\left(-\ln^2(a/a_0)/2s^2\right), \quad (12)$$

with  $s = 0.92$  and  $a_0 = 0.3 \mu\text{m}$ . The refractive index of this aerosol is 1.385. The Mie code provided by Mishchenko *et al.* [67] is used to calculate the scattering matrix of this aerosol model. Kokhanovsky *et al.* [60] have also provided the tabular data for the aerosol scattering matrix, which we confirmed to be the same as the Mie code output.

The Rayleigh phase matrix is [80]

$$\mathbf{P}_R(\Theta) = \frac{3}{4} \times \begin{pmatrix} 1 + \cos^2\Theta & -\sin^2\Theta & 0 & 0 \\ -\sin^2\Theta & 1 + \cos^2\Theta & 0 & 0 \\ 0 & 0 & 2 \cos \Theta & 0 \\ 0 & 0 & 0 & 2 \cos \Theta \end{pmatrix}, \quad (13)$$

where the first element  $P_{11}$  is the phase function, normalized to  $4\pi$ . The nonconservative case configuration is the same as the conservative case, except that a gas absorption is added. The gas absorption optical depth is set to be the same as the Rayleigh scattering optical depth so that the Rayleigh single-scattering albedo is 0.5. The ground reflection albedo is zero for both cases.

The designed cases are solved by both IMS and EMS. For IMS, Eqs. (4)–(6) are used to mix scattering properties, and then the SOS method is used to calculate the radiation field at both the top and bottom of the atmospheric turbid medium. The Gaussian quadrature number of 120 is used for viewing zenith angle integration. We have tested that a higher Gaussian quadrature term did not change the results. The optical depth integration step is  $10^{-3}$ , which is unusually small due to the need to ensure extremely accurate solutions. With these configurations, the time required to achieve convergence is 18 h 30 min, on a system with 2.7 GHz Intel Core i5 and memory of 16 GB 1600 MHz DDR3. In the case of EMS, the MC code is used to handle the mixture explicitly, as described earlier. In order to achieve simulations with negligible statistical noise, the number of photon packages entering the medium is taken as  $5 \times 10^7$ . The time required to achieve convergence for MC is 10 h 3 min running on the same computer mentioned above.

After the radiation field is obtained with both IMS and EMS, the Stokes parameters are compared to confirm the equivalence of the two schemes. Figure 2 shows the Stokes parameters at TOA as a function of the viewing zenith angle for the conservative case calculated with both schemes. In the figures, the IMS and EMS results are represented by the SOS and MC labels, respectively. The solar zenith angle is  $60^\circ$ , and three viewing azimuth angles are shown:  $\phi = 0^\circ, 90^\circ$ , and  $180^\circ$ . It is found that results from the two mixture schemes agree with each other very well. Figure 3 shows differences between the Stokes parameters calculated with the two schemes. To quantify the comparison, radiance percentage difference  $\eta$  and mean percentage difference  $\bar{\eta}$  are calculated as follows:

$$\eta = 100 \times (I_{\text{SOS}} - I_{\text{MC}}) / I_{\text{MC}}, \quad (14)$$

$$\bar{\eta} = \sum_{i=1}^N |\eta_i| / N, \quad (15)$$

where  $N$  is the number of viewing zenith angles, and  $|\eta_i|$  takes the absolute value of  $\eta_i$ . The maximum percentage differences of the TOA radiance are around 0.054%, and the mean



percentage differences are around 0.018%. Table 1 summarizes the maximum and mean radiance differences for all cases studied in this paper. The polarization elements also agree with each other well. The differences of  $Q/I$ ,  $U/I$ , and  $V/I$  between the two methods are on the order of  $10^{-4}$  for TOA. The maximum differences happen around the viewing zenith angle  $90^\circ$ , where it is difficult to achieve high accuracy for the MC simulations [50].

Figures 4 and 5 are the same as Figs. 2 and 3 except that they are for BOA. It is shown that the maximum percentage difference is around 0.08% for BOA, and the mean percentage difference  $\bar{\eta}$  is 0.03%. The polarized element difference at the bottom is similar to the top. These differences are smaller or close to the smallest difference shown in the aerosol column of Table 1 in Kokhanosky *et al.* [60]. The angular variation of the agreement between MC and SOS shows no systematic pattern, both for the TOA and BOA cases. The extremely small difference of the Stokes parameters between the two mixture schemes shows that we have successfully demonstrated the equivalence of the two schemes to the accuracy level of the vector radiative transfer benchmark.

To test the impact of absorption, our experiment is extended to the nonconservative scattering medium condition. In this case, a gas absorption is added to Rayleigh particles. The single-scattering albedo of Rayleigh particles is taken as 0.5, and the Rayleigh optical depth is  $\tau_{er} = 0.5^{-1} \times 0.3186 = 0.6372$ . This way, the Rayleigh scattering optical depth has been kept the same as the conservative case. All other system configurations are the same as the conservative case, including the aerosol model and surface reflection albedo. The number of photons are taken as  $5 \times 10^7$  in the MC code, as was done in the conservative case. The time taken to converge for both MC and SOS is similar to the conservative case.

Figure 6 shows the Stokes parameters at TOA for the nonconservative case calculated by IMS (SOS) and EMS (MC). Figure 7 shows differences in the Stokes parameters between the two schemes. Figures 8 and 9 are the same as Figs. 6 and 7, except that these are for the bottom of the nonconservative medium. It is observed that the maximum percentage differences of the radiance are around 0.053% for TOA and 0.12% for BOA. The mean percentage differences of the radiance are around 0.021% for TOA and 0.024% for BOA, respectively. The differences of  $Q/I$ ,  $U/I$ , and  $V/I$  between the two schemes are on the order of  $10^{-4}$  for both the TOA and BOA. The differences observed for the nonconservative case are consistent with those of the conservative case. In addition, these differences are smaller than most practical accuracy requirements of the radiative transfer simulations. Thus, we can safely conclude that one can use IMS for calculating radiative transfer for multiple scatterers in turbid media.

## 4. CONCLUSION

This paper successfully demonstrates the equivalence of two mixture schemes of optical properties of multiple scatterers in vector radiative transfer models. In the EMS, Rayleigh and aerosol particles are mixed based on the scattering probability determined by their individual optical depths and phase matrices using the MC method [50]. On the other hand, the IMS calculates the effective optical properties of the mixed medium by averaging the optical properties of each scatterer weighted by their optical depths; then the averaged

optical properties are input into the SOS code [48]. The comparison of the Stokes vector elements is done for both the top and bottom of the considered turbid media; one is conservative and the other has gas absorption included in molecular interaction.

It has been found that the radiances calculated by these two procedures show a maximum difference of 0.055% for reflected radiances, and 0.08% for transmitted radiances, for the conservative medium conditions. The differences of  $Q/I$ ,  $U/I$ , and  $V/I$  are of the order of  $10^{-4}$  for both TOA and BOA. For the nonconservative medium, the two procedures show a maximum difference of 0.053% for the reflected radiance, and 0.12% for the transmitted radiance. The differences of  $Q/I$ ,  $U/I$ , and  $V/I$  are at a similar level as the conservative case. The observed differences for the polarized radiation field are smaller than general accuracy requirements of numerical solutions for practical applications. Therefore, for practical purposes, the equivalence of the two mixture schemes is demonstrated. This result has important implications for many applications using the radiative transfer theory. One example is the atmospheric correction for ocean color remote sensing, in which an aerosol lookup table has to be built, which involves a mixture of Rayleigh and aerosol particles. There have been debates in the community on the validity of the IMS used in the radiative transfer simulation. This work fully demonstrates that it is appropriate to use IMS for this and other similar applications.

## Acknowledgments

This study is partially supported by the NASA Radiation Science program administered by Hal Maring and the Biology and Biogeochemistry program administered by Paula Bontempi. The authors also thank Science System Applications Inc. for contractual support.

**Funding.** National Aeronautics and Space Administration (NASA) (NNX15AB94G, NNX15AL87G).

## References

1. Chandrasekhar, S. Dover Books on Intermediate and Advanced Mathematics. Dover Publications; 1960. Radiative Transfer.
2. van de Hulst, HC. Dover Books on Physics. Dover Publications; 1981. Light Scattering by Small Particles. reprint ed
3. Mishchenko, MI., Travis, LD. Electromagnetic Scattering by Nonspherical Particles. Springer; 2003. p. 77-127.
4. Brown AJ, Xie Y. Symmetry relations revealed in Mueller matrix hemispherical maps. J Quant Spectrosc Radiat Transfer. 2012; 113:644–651.
5. Mobley, CD. Light and Water: Radiative Transfer in Natural Waters. Academic; 1994.
6. Liou, KN. An Introduction to Atmospheric Radiation. 2nd. Vol. 84. Academic; 2002. of International Geophysics Series
7. Stamnes K, Tsay SC, Wiscombe W, Jayaweera K. Numerically stable algorithm for discrete-ordinate-method radiative transfer in multiple scattering and emitting layered media. Appl Opt. 1988; 27:2502–2509. [PubMed: 20531783]
8. Weng F. A multi-layer discrete-ordinate method for vector radiative transfer in a vertically-inhomogeneous, emitting and scattering atmosphere—I. Theory. J Quant Spectrosc Radiat Transfer. 1992; 47:19–33.
9. Weng F. A multi-layer discrete-ordinate method for vector radiative transfer in a vertically-inhomogeneous, emitting and scattering atmosphere—II. Application. J Quant Spectrosc Radiat Transfer. 1992; 47:35–42.

10. Sánchez A, Smith T, Krajewski W. A three-dimensional atmospheric radiative transfer model based on the discrete-ordinates method. *Atmos Res.* 1994; 33:283–308.
11. Haferman JL, Smith TF, Krajewski WF. A multi-dimensional discrete-ordinates method for polarized radiative transfer. Part I: validation for randomly oriented axisymmetric particles. *J Quant Spectrosc Radiat Transfer.* 1997; 58:379–398.
12. Schulz F, Stamnes K, Weng F. VDISORT: an improved and generalized discrete ordinate method for polarized (vector) radiative transfer. *J Quant Spectrosc Radiat Transfer.* 1999; 61:105–122.
13. Siewert C. A discrete-ordinates solution for radiative-transfer models that include polarization effects. *J Quant Spectrosc Radiat Transfer.* 2000; 64:227–254.
14. Spurr RJ. VLIDORT: a linearized pseudo-spherical vector discrete ordinate radiative transfer code for forward model and retrieval studies in multilayer multiple scattering media. *J Quant Spectrosc Radiat Transfer.* 2006; 102:316–342.
15. Rozanov V, Rozanov A, Kokhanovsky A, Burrows J. Radiative transfer through terrestrial atmosphere and ocean: software package SCIATRAN. *J Quant Spectrosc Radiat Transfer.* 2014; 133:13–71.
16. Ambartsumian VA. A new method for computing light scattering in turbid media. *Izv Akad Nauk SSSR, Ser Geogr Geofiz.* 1942; 3:97–104.
17. Ambartsumian, VA. *Theoretical Astrophysics.* Pergamon; 1958.
18. Adams C, Kattawar G. Solutions of the equations of radiative transfer by an invariant imbedding approach. *J Quant Spectrosc Radiat Transfer.* 1970; 10:341–356.
19. Mishchenko MI. Reflection of polarized light by plane-parallel slabs containing randomly-oriented, nonspherical particles. *J Quant Spectrosc Radiat Transfer.* 1991; 46:171–181.
20. Mishchenko MI, Travis LD. Satellite retrieval of aerosol properties over the ocean using polarization as well as intensity of reflected sunlight. *J Geophys Res Atmos.* 1997; 102:16989–17013.
21. Stokes GG. On the intensity of the light reflected from or transmitted through a pile of plates. *Proc R Soc London.* 1860; 11:545–556.
22. Hansen JE. Multiple scattering of polarized light in planetary atmospheres part II. Sunlight reflected by terrestrial water clouds. *J Atmos Sci.* 1971; 28:1400–1426.
23. De Haan JF, Bosma PB, Hovenier JW. The adding method for multiple scattering calculations of polarized light. *Astron Astrophys.* 1987; 183:371–391.
24. Plass GN, Kattawar GW, Catchings FE. Matrix operator theory of radiative transfer. 1: Rayleigh scattering. *Appl Opt.* 1973; 12:314–329. [PubMed: 20125285]
25. Kattawar GW, Plass GN, Catchings FE. Matrix operator theory of radiative transfer. 2: scattering from maritime haze. *Appl Opt.* 1973; 12:1071–1084. [PubMed: 20125470]
26. Waterman PC. Matrix-exponential description of radiative transfer. *J Opt Soc Am.* 1981; 71:410–422.
27. Nakajima T, Tanaka M. Effect of wind-generated waves on the transfer of solar radiation in the atmosphere-ocean system. *J Quant Spectrosc Radiat Transfer.* 1983; 29:521–537.
28. Fischer J, Grassl H. Radiative transfer in an atmosphere-ocean system: an azimuthally dependent matrix-operator approach. *Appl Opt.* 1984; 23:1032–1039. [PubMed: 18204679]
29. Liu Q, Ruprecht E. Radiative transfer model: matrix operator method. *Appl Opt.* 1996; 35:4229–4237. [PubMed: 21102832]
30. Hollstein A, Fischer J. Radiative transfer solutions for coupled atmosphere ocean systems using the matrix operator technique. *J Quant Spectrosc Radiat Transfer.* 2012; 113:536–548.
31. Sanghavi S, Davis AB, Eldering A. vSmartMOM: a vector matrix operator method-based radiative transfer model linearized with respect to aerosol properties. *J Quant Spectrosc Radiat Transfer.* 2014; 133:412–433.
32. Kourganoff, V. *Basic Methods in Transfer Problems.* Clarendon; 1952.
33. Garcia R, Siewert C. A generalized spherical harmonics solution for radiative transfer models that include polarization effects. *J Quant Spectrosc Radiat Transfer.* 1986; 36:401–423.

34. Ustinov E. Methods of spherical harmonics. Application to the transfer of polarized radiation in a vertically nonuniform planetary atmosphere. *Mathematical apparatus. Cosmic Res.* 1989; 26:473–484.
35. Evans KF. The spherical harmonics discrete ordinate method for three-dimensional atmospheric radiative transfer. *J Atmos Sci.* 1998; 55:429–446.
36. Evans KF. SHDOMPPDA: a radiative transfer model for cloudy sky data assimilation. *J Atmos Sci.* 2007; 64:3854–3864.
37. Myneni R, Asrar G, Kanemasu E. Light scattering in plant canopies: the method of successive orders of scattering approximations (SOSA). *Agric For Meteorol.* 1987; 39:1–12.
38. Lenoble, J. Radiative Transfer, Studies in Geophysical Optics and Remote Sensing. Deepak Publications; 1993.
39. Chami M, Santer R, Dilligeard E. Radiative transfer model for the computation of radiance and polarization in an ocean-atmosphere system: polarization properties of suspended matter for remote sensing. *Appl Opt.* 2001; 40:2398–2416. [PubMed: 18357248]
40. Min Q, Duan M. A successive order of scattering model for solving vector radiative transfer in the atmosphere. *J Quant Spectrosc Radiat Transfer.* 2004; 87:243–259.
41. Duan M, Min Q. A semi-analytic technique to speed up successive order of scattering model for optically thick media. *J Quant Spectrosc Radiat Transfer.* 2005; 95:21–32.
42. Greenwald T, Bennartz R, O'Dell C, Heidinger A. Fast computation of microwave radiances for data assimilation using the "successive order of scattering" method. *J Appl Meteorol.* 2005; 44:960–966.
43. Heidinger AK, O'Dell C, Bennartz R, Greenwald T. The successive-order-of-interaction radiative transfer model. Part I: model development. *J Appl Meteorol Climatol.* 2006; 45:1388–1402.
44. Kotchenova SY, Vermote EF, Matarrese R, Klemm FJ Jr. Validation of a vector version of the 6S radiative transfer code for atmospheric correction of satellite data. Part I: path radiance. *Appl Opt.* 2006; 45:6762–6774. [PubMed: 16926910]
45. Kotchenova SY, Vermote EF. Validation of a vector version of the 6S radiative transfer code for atmospheric correction of satellite data. Part II. Homogeneous Lambertian and anisotropic surfaces. *Appl Opt.* 2007; 46:4455–4464. [PubMed: 17579701]
46. Lenoble J, Herman M, Deuzé J, Lafrance B, Santer R, Tanré D. A successive order of scattering code for solving the vector equation of transfer in the earth's atmosphere with aerosols. *J Quant Spectrosc Radiat Transfer.* 2007; 107:479–507.
47. Suzuki T, Nakajima T, Tanaka M. Scaling algorithms for the calculation of solar radiative fluxes. *J Quant Spectrosc Radiat Transfer.* 2007; 107:458–469.
48. Zhai PW, Hu Y, Trepte CR, Lucker PL. A vector radiative transfer model for coupled atmosphere and ocean systems based on successive order of scattering method. *Opt Express.* 2009; 17:2057–2079. [PubMed: 19219111]
49. Zhai P-W, Hu Y, Chowdhary J, Trepte CR, Lucker PL, Josset DB. A vector radiative transfer model for coupled atmosphere and ocean systems with a rough interface. *J Quant Spectrosc Radiat Transfer.* 2010; 111:1025–1040.
50. Zhai P-W, Kattawar GW, Yang P. Impulse response solution to the three-dimensional vector radiative transfer equation in atmosphere-ocean systems. I. Monte Carlo method. *Appl Opt.* 2008; 47:1037–1047. [PubMed: 18327274]
51. Plass GN, Kattawar GW. Monte Carlo calculations of light scattering from clouds. *Appl Opt.* 1968; 7:415–419. [PubMed: 20068603]
52. Kattawar GW, Plass GN. Radiance and polarization of multiple scattered light from haze and clouds. *Appl Opt.* 1968; 7:1519–1527. [PubMed: 20068833]
53. Marchuk, GI., Mikhailov, GA., Nazareliev, M., Darbinjan, RA., Kargin, BA., Elepov, BS. of Springer Series in Optical Sciences. Vol. 12. Springer; 2013. The Monte Carlo Methods in Atmospheric Optics.
54. Kattawar, GW. Selected Papers on Multiple Scattering in Plane Parallel Atmospheres and Oceans: Methods. Society of Photo Optical; 1991.
55. Roberti L, Kummerow C. Monte Carlo calculations of polarized microwave radiation emerging from cloud structures. *J Geophys Res Atmos.* 1999; 104:2093–2104.

56. Tynes HH, Kattawar GW, Zege EP, Katsev IL, Prikhach AS, Chaikovskaya LI. Monte Carlo and multicomponent approximation methods for vector radiative transfer by use of effective Mueller matrix calculations. *Appl Opt.* 2001; 40:400–412. [PubMed: 18357013]
57. O'Brien D. Accelerated quasi Monte Carlo integration of the radiative transfer equation. *J Quant Spectrosc Radiat Transfer.* 1992; 48:41–59.
58. Preisendorfer, RW. of International Series of Monographs in Pure and Applied Mathematics. Vol. 74. Elsevier; 2014. Radiative Transfer on Discrete Spaces.
59. Marshak, A., Davis, A. 3D Radiative Transfer in Cloudy Atmospheres. Springer; 2005.
60. Kokhanovsky AA, Budak VP, Cornet C, Duan M, Emde C, Katsev IL, Klyukov DA, Korkin SV, C-Labonnote L, Mayer B. Benchmark results in vector atmospheric radiative transfer. *J Quant Spectrosc Radiat Transfer.* 2010; 111:1931–1946.
61. Brown AJ. Equivalence relations and symmetries for laboratory, LIDAR, and planetary Müller matrix scattering geometries. *J Opt Soc Am A.* 2014; 31:2789–2794.
62. Hu Y-X, Winker D, Yang P, Baum B, Poole L, Vann L. Identification of cloud phase from PICASSO-CENA LIDAR depolarization: a multiple scattering sensitivity study. *J Quant Spectrosc Radiat Transfer.* 2001; 70:569–579.
63. Hammad A, Chapman S. VII. The primary and secondary scattering of sunlight in a plane-stratified atmosphere of uniform composition. *London Edinburgh Dublin Philos Mag J Sci.* 1939; 28(186):99–110.
64. Lenoble, J. of Studies in Geophysical Optics and Remote Sensing. Vol. 1. A. Deepak Hampton; 1985. Radiative Transfer in Scattering and Absorbing Atmospheres: Standard Computational Procedures.
65. Wiscombe W. The delta-M method: rapid yet accurate radiative flux calculations for strongly asymmetric phase functions. *J Atmos Sci.* 1977; 34:1408–1422.
66. Hu Y-X, Wielicki B, Lin B, Gibson G, Tsay S-C, Stamnes K, Wong T.  $\delta$ -Fit: a fast and accurate treatment of particle scattering phase functions with weighted singular-value decomposition least-squares fitting. *J Quant Spectrosc Radiat Transfer.* 2000; 65:681–690.
67. Mishchenko, MI., Travis, LD., Lacis, AA. Scattering, Absorption, and Emission of Light by Small Particles. Cambridge University; 2002.
68. Sanghavi S, Natraj V. Using analytic derivatives to assess the impact of phase function Fourier decomposition technique on the accuracy of a radiative transfer model. *J Quant Spectrosc Radiat Transfer.* 2013; 119:137–149.
69. Zhai P-W, Hu Y, Josset DB, Trepte CR, Lucker PL, Lin B. Exact first order scattering correction for vector radiative transfer in coupled atmosphere and ocean systems. *Proc SPIE.* 2012; 8364:83640A.
70. Schulz F, Stamnes K. Angular distribution of the Stokes vector in a plane-parallel, vertically inhomogeneous medium in the vector discrete ordinate radiative transfer (VDISORT) model. *J Quant Spectrosc Radiat Transfer.* 2000; 65:609–620.
71. Zhai P-W, Hu Y, Josset DB, Trepte CR, Lucker PL, Lin B. Advanced angular interpolation in the vector radiative transfer for coupled atmosphere and ocean systems. *J Quant Spectrosc Radiat Transfer.* 2013; 115:19–27.
72. Zhai P-W, Hu Y, Winker DM, Franz BA, Boss E. Contribution of Raman scattering to polarized radiation field in ocean waters. *Opt Express.* 2015; 23:A582–A596. [PubMed: 26072883]
73. Coulson KL, Dave JV, Sckera Z. Tables Related to Radiation Emerging from a Planetary Atmosphere with Rayleigh Scattering (California University. 1960
74. Chowdhary J, Cairns B, Travis LD. Contribution of water-leaving radiances to multiangle, multispectral polarimetric observations over the open ocean: bio-optical model results for case 1 waters. *Appl Opt.* 2006; 45:5542–5567. [PubMed: 16855652]
75. Cahalan RF, Ridgway W, Wiscombe WJ, Gollmer S. Independent pixel and Monte Carlo estimates of stratocumulus albedo. *J Atmos Sci.* 1994; 51:3776–3790.
76. Battaglia A, Mantovani S. Forward Monte Carlo computations of fully polarized microwave radiation in non-isotropic media. *J Quant Spectrosc Radiat Transfer.* 2005; 95:285–308.
77. Chen Y, Liou K. A Monte Carlo method for 3D thermal infrared radiative transfer. *J Quant Spectrosc Radiat Transfer.* 2006; 101:166–178.

78. Tomasi C, Vitale V, Petkov B, Lupi A, Cacciari A. Improved algorithm for calculations of Rayleigh-scattering optical depth in standard atmospheres. *Appl Opt.* 2005; 44:3320–3341. [PubMed: 15943269]
79. Brown AJ. Spectral bluing induced by small particles under the Mie and Rayleigh regimes. *Icarus.* 2014; 239:85–95.
80. Wendisch, M., Yang, P. *Theory of Atmospheric Radiative Transfer.* Wiley; 2012.

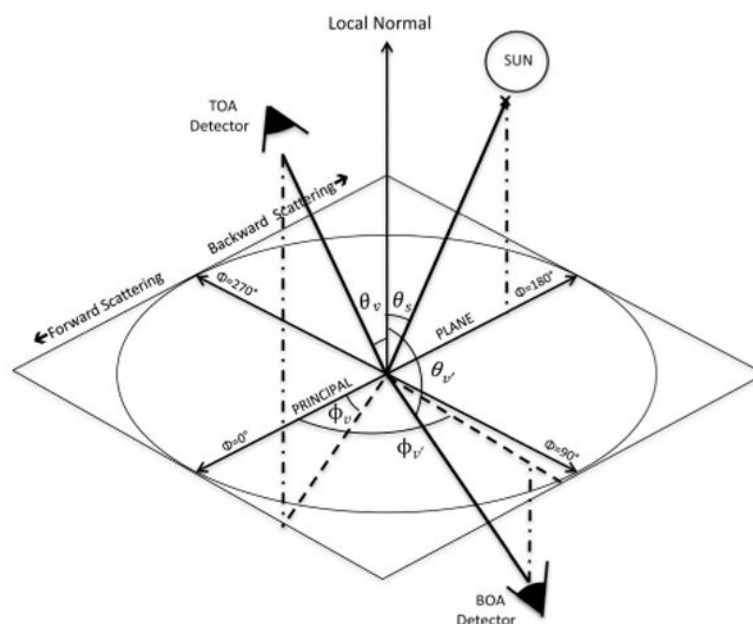


**Fig. 1.** Diagram of the solar and viewing angle geometry. The local normal vector and the Sun define the principal plane. Two detectors are shown: one is at the TOA, measuring the reflected Stokes parameters; the other is at the BOA, measuring the transmitted Stokes parameters.

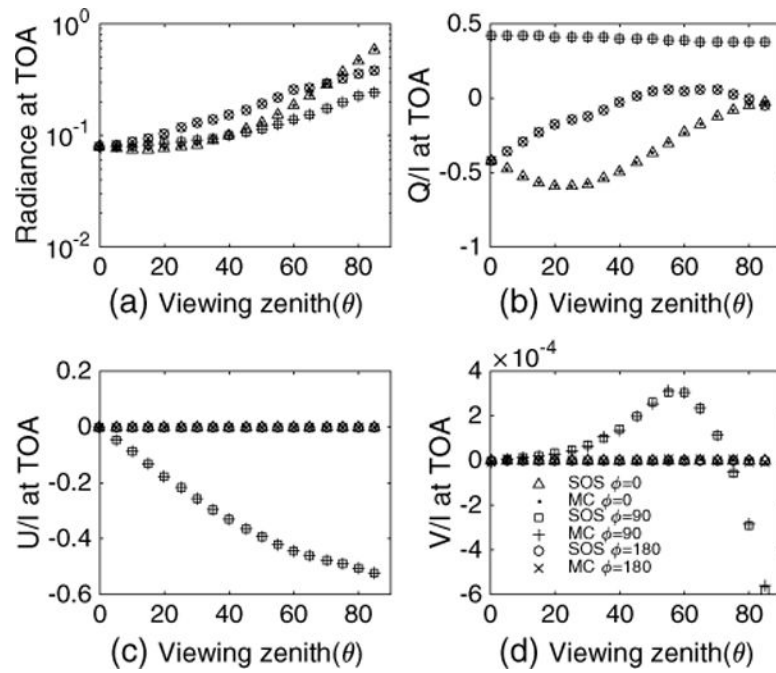
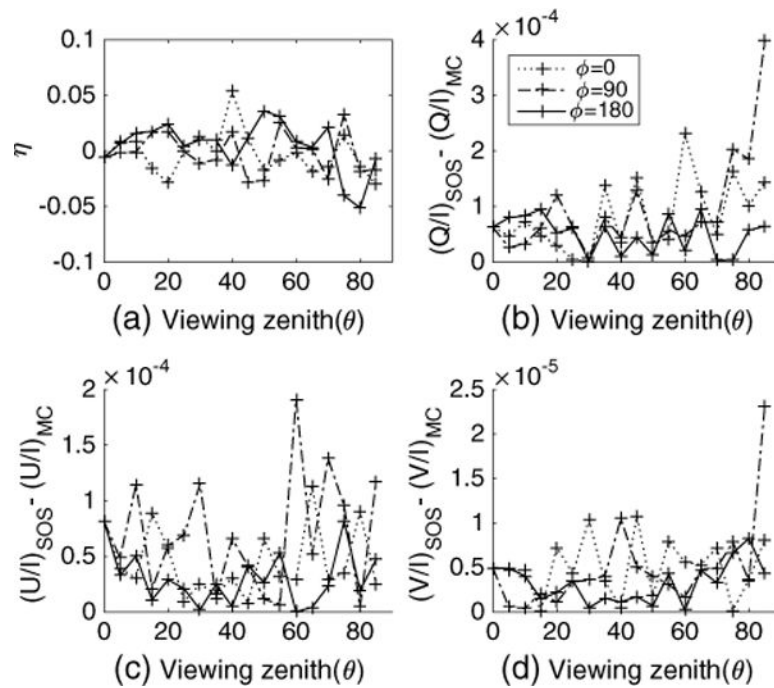


Fig. 2.

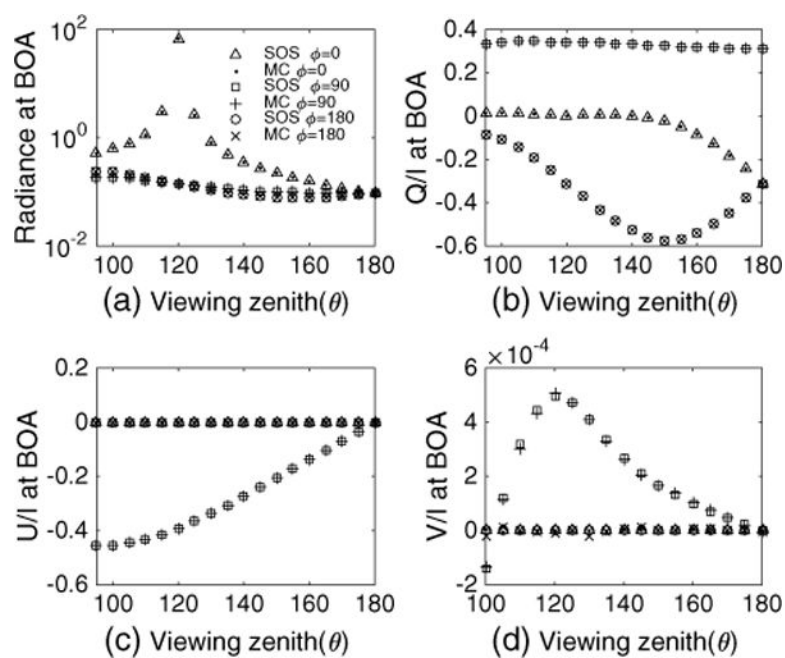
Radiance  $I$  and  $Q/I$ ,  $U/I$ , and  $V/I$  at TOA for the conservative case. The azimuth angle  $\phi$  legend in Fig. 2(d) applies to all four subplots in Fig. 2. The solar zenith angle is 60°.



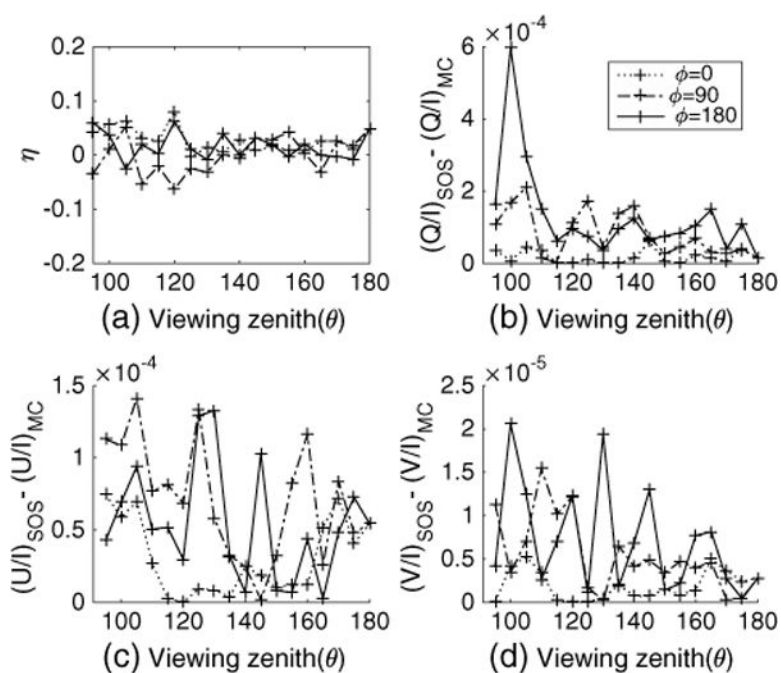


**Fig. 3.**

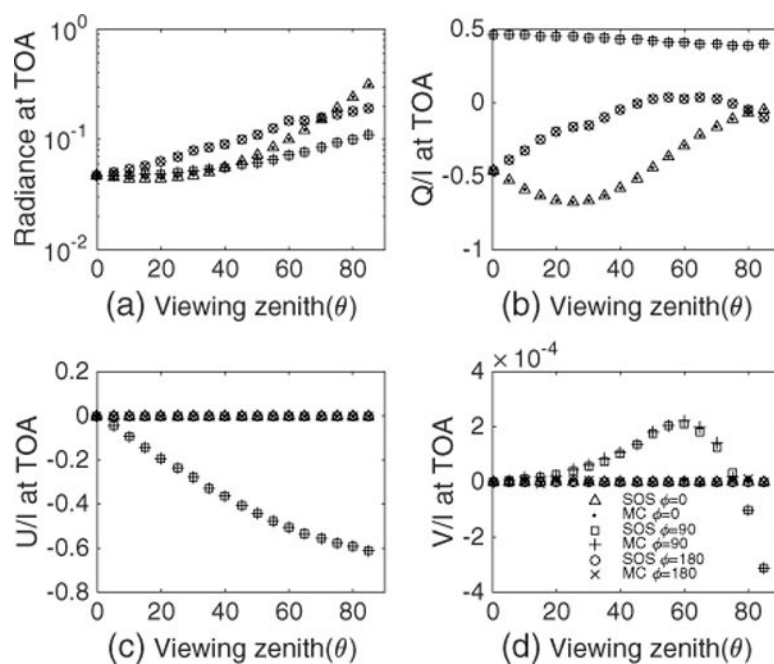
Radiance percentage difference between the SOS and MC methods at TOA for the conservative case shown as in Fig. 2. Also shown are the  $Q/I$ ,  $U/I$ , and  $V/I$  differences between the SOS and MC methods. The azimuth angle  $\phi$  legend in Fig. 3(d) applies to all four subplots in Fig. 3.



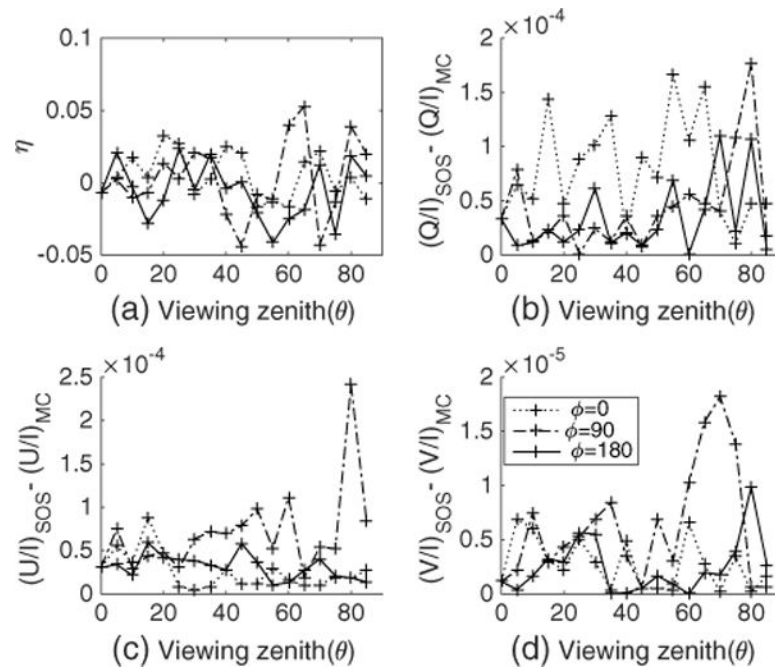
**Fig. 4.**  
Same as Fig. 2 except that these are for the BOA.



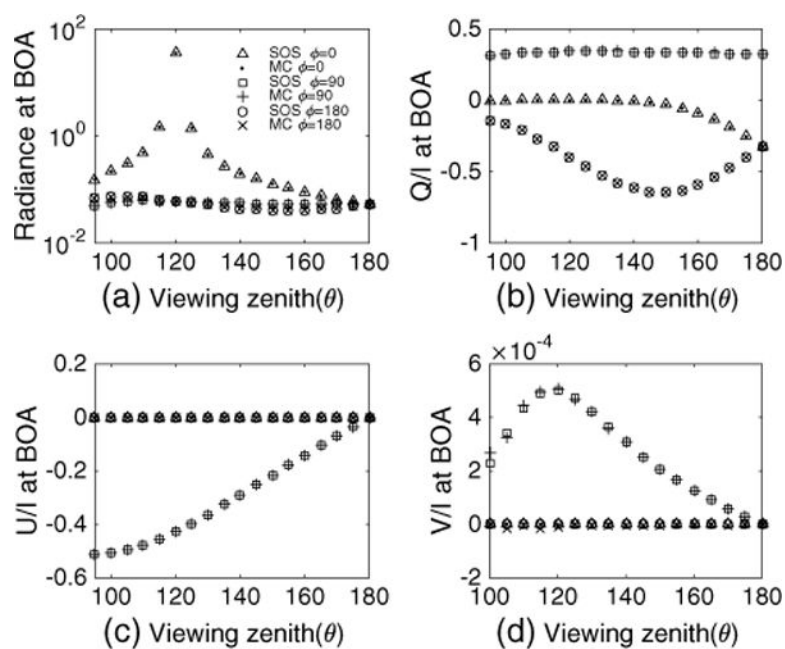
**Fig. 5.**  
Same as Fig. 3 except that these are for the BOA.



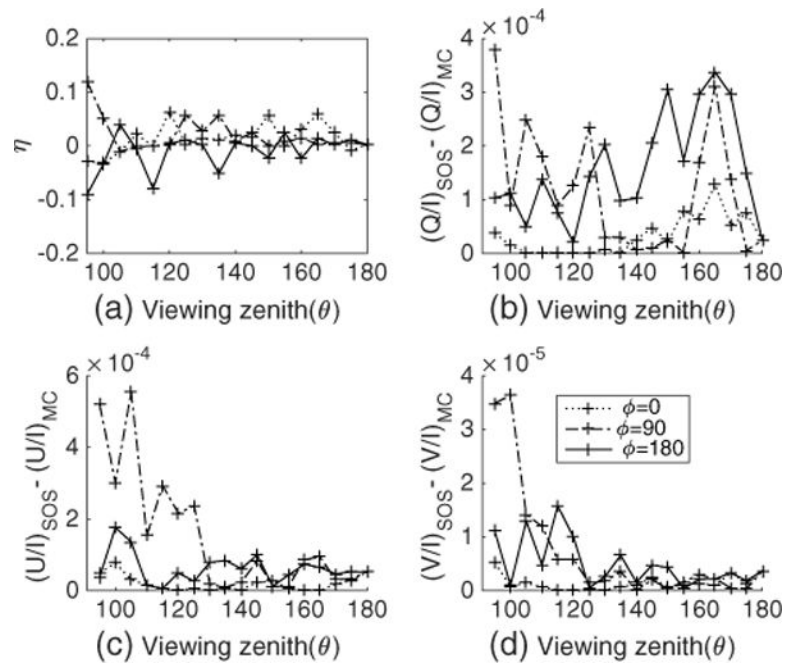
**Fig. 6.**  
Radiation field at TOA for the nonconservative (absorbing) case.

**Fig. 7.**

Differences between the radiation field calculated by the two methods for case shown in Fig. 6.



**Fig. 8.**  
Radiation field at the BOA for the nonconservative case.

**Fig. 9.**

Difference between the radiation field calculated by the two methods at the BOA for the nonconservative case.

**Table 1**  
Maximum and Mean Values of the Percentage Differences for Two Mixing Schemes

Azimuth Angles	Conservative				Nonconservative			
	TOA		BOA		TOA		BOA	
	Max	Mean	Max	Mean	Max	Mean	Max	Mean
0°	0.054	0.015	0.080	0.028	0.033	0.014	0.064	0.023
90°	0.033	0.014	0.063	0.030	0.053	0.021	0.12	0.022
180°	0.051	0.018	0.062	0.022	0.041	0.018	0.091	0.024